Carbohydrate Polymers 102 (2014) 317–323

Contents lists available at ScienceDirect

Carbohydrate Polymers

journal homepage: www.elsevier.com/locate/carbpol

A novel polymer based on $MtCu^{2+}$/cellulose acetate with antimicrobial activity

J.E. Bruna*, M.J. Galotto, A. Guarda, F. Rodríguez

Food Packaging Laboratory (Laben-Chile), Department of Science and Food Technology, Faculty of Technology, Center for the Development of Nanoscience and Nanotechnology (CEDENNA), Universidad de Santiago de Chile (USACH), Santiago, Chile

ARTICLE INFO

Article history:
Received 2 August 2013
Received in revised form
16 November 2013
Accepted 26 November 2013
Available online 4 December 2013

Keywords:
Montmorillonite
Copper
Antimicrobial activity
Copper modified clay
Cellulose acetate
Nanocomposites

ABSTRACT

Cellulose acetate (CA)/copper montmorillonite modified ($MtCu^{2+}$) antimicrobial nanocomposites for food packaging containing 1, 3 and 5 wt.% nanoparticles were prepared by solution casting technique. X-ray diffraction (XRD) and transmission electron microscopy revealed the existence of intercalated and no intercalated clay form in the CA matrix. The thermal stability of the $MtCu^{2+}$/CA nanocomposites was measured by TGA and DSC, which indicated that the nanocomposites were less thermally stable in comparison to CA pure. Mechanical testing of material did not show differences when $MtCu^{2+}$ was added in CA. On the other hand, antimicrobial effect was observed for nanocomposites films, obtaining a 98% reduction against *Escherichia coli*.

1. Introduction

Polymers have replaced conventional materials in packaging applications such as paper and paperboard, metal and glass, due to their functionality, lightweight, ease of processing, and low cost (Risch, 2009). Thus, thermoplastic like polyolefins (polyethylene, PE and polypropylene, PP), polyethylene terephthalate (PET), polyvinyl chloride (PVC), and polyamides are the most used by this industry (Rodríguez, Galotto, Guarda, & Bruna, 2012).

However, despite their enormous versatility, most of polymer materials are non-biodegradable which has generated an important environmental problem (Pillai & Luckachan, 2011), causing not only air pollution and underground water contamination, but also adds to global warming or to the "greenhouse effect", which are harmful to human and animal life (Yoksan & Yokesahachart, 2011).

This has led to the use of new products based on biodegradable polymers of natural and synthetic origin as an alternative to non-biodegradable polymers (Pillai & Luckachan, 2011).

Cellulose acetate (CA) is a biodegradable polymer derived from cellulose, which is one of the most abundant polysaccharide on earth (Rimdusit, Jingjid, Damrongsakkul, Tiptipakorn, & Takeichi, 2008), which is synthesized by the reaction of acetic anhydride with cotton liners or wood pulp. CA is used to produce clear adhesive tape, tool handles, eyeglass frames, textiles and related materials because of its relatively low cost, draping quality, softness, comfort, luster, and natural feel (Mohanty, Park, Misra, & Drzal, 2004). Moreover, it is being used in medical applications, such as membrane material for desalination, while other cellulose derivatives, such as cellulose acetate butyrate are being used in capsule form as drug-releasing purposes (Hoenich, 2006).

CA degradation can be produced by biological, chemical, and photochemical mechanism, but the combination of photo and biodegradation allows a synergy that enhances the overall degradation rate (Puls, Wilson & Holter, 2011).

Unfortunately, the use of biodegradable polymers has been limited due to their poor mechanical and barrier properties. So, the use of nanoparticles could be an alternative to improve these deficiencies. These new nanocomposites would allow to produce eco-friendly materials (Sozer & Kokini, 2009) and also may increase their barrier properties to gases (Arora & Padua, 2010). In this way the use of clays in biopolymers has allowed to obtain materials with improved barrier properties (Choudalakis & Gotsis, 2009) and enhance their mechanical properties maintaining their biodegradability (Tang, Kumar, Alavi & Sandeep, 2012) thus being able replace the conventional polymers.

On the other hand, in recent years food packaging has evolved from simply a container to hold food to something today that can

* Corresponding author. Tel.: +56 2 7184520.
E-mail address: julio.bruna@usach.cl (J.E. Bruna).

0144-8617/$ – see front matter © 2013 Elsevier Ltd. All rights reserved.
http://dx.doi.org/10.1016/j.carbpol.2013.11.038

play an active role in food quality (Risch, 2009) in order to increase the shelf life of packaged food.

Active packaging systems are successfully used to increase the shelf life of processed foods and can be categorized into adsorbing and releasing systems (for example, oxygen scavengers, ethylene scavengers, liquid and moisture absorbers, flavor and odor absorbers or releasers, antimicrobials, etc.) (Abreu, Cruz, & Losada, 2012). Among the active packaging systems are those which release antimicrobial agents into food surface, where microbial growth predominates, inhibiting or retarding microbial growth and food spoilage (de Azeredo, 2013).

In order to develop antimicrobial food packaging, different types of antimicrobial agents have been used, where it can highlight the use of which contains high concentrations of essentials oil derivatives such as carvacrol, eugenol, cinnamaldehyde and thymol (Quintero, Rodriguez, Bruna, Guarda, & Galotto, 2012), organics acids such as sorbic acid (Hauser & Wunderlicha, 2011) and Benzoic acid (Cruz-Romero, Murphy, Morris, Cummins, & Kerry, 2013) and some metal ions, such as silver, copper and zinc, which possess antibacterial and antifungal properties (Malachova, Praus, Rybkova, & Kozak, 2011).

Copper has been of particular interest because, unlike other antimicrobial metals, it presents a broad spectrum of action against bacteria and molds, (Bruna, Peñaloza, Guarda, Rodríguez & Galotto, 2012) due to its ability to accept or donate electrons, thus having high levels of catalytic oxidation and a high reduction potential (Nan et al., 2008).

A new material based on cellulose acetate (CA) biopolymer with antimicrobial activity, using montmorillonite modified with copper ($MtCu^{2+}$) by ion exchange was developed in this research, in order to obtain a material with modified properties with the aid of nanofillers and copper and also reducing the use of non-degradable materials using an eco-friendly materials like cellulose acetate.

The aim of this study was to evaluate the effect $MtCu^{2+}$ on the properties of nanocomposites. The nanocomposites thus elaborated were characterized by X-ray diffraction (XRD), differential scanning calorimetry (DSC), thermo gravimetric analysis (TGA), oxygen permeability, optical properties, tensile test, scanning electron microscopy (SEM) and antibacterial properties.

2. Experimental

2.1. Materials

Cellulose acetate (CA) (39.8 wt.% acetyl content with number average molecular weight: 30,000), Aldrich, natural montmorillonite (Mt), purchased from Southern Clay Products, under the trade name of Cloisite® Na^+, Cupric sulfate pentahydrate ($CuSO_4 \times 5H_2O$), 99.995% trace metals, Aldrich, triethyl citrate (TEC, Triethyl Citrate, 99% (FCC, FG), SAFC, Luria-Bertani (Muffler & Ulber) medium for bacteria were used in this study, *Escherichia coli* O157:H7 n/t obtained from the Public Health Institute, ISP (Santiago, Chile)

2.2. Modified clay preparation

The modification of $MtNa^+$ was carried out in a $CuSO_4$ solution by ion exchange according to early works (Bruna et al., 2012), obtaining $MtCu^{2+}$ sizes < 75 μm.

2.3. $MtCu^{2+}$/CA nanocomposites preparation

$MtCu^{2+}$/CA nanocomposites were prepared in solution by casting technique, for this the required amounts of CA and triethyl citrate (as plasticizer) were dissolved in acetone under vigorous stirring for 1 h at ambient temperature. In parallel, $MtCu^{2+}$ was dispersed in acetone and sonicated, during 1 h at room temperature. The CA solution was then added on $MtCu^{2+}$ suspension under vigorous stirring. This mixture was stirred and then sonicated, during 1 h at room temperature. The nanocomposite was poured on a Petri dish and left to dry at 40 °C (Rodríguez et al., 2011), obtaining nanocomposite blends with 1, 3 and 5 wt.% of $MtCu^{2+}$, maintaining a constant concentration (5 wt.%) of plasticizer of in all cases.

2.4. Characterization

2.4.1. X-ray diffraction

X-ray diffraction patterns of the nanocomposites were recorded at room temperature, on a Siemens D5000 diffractometer (Munich, Germany) with Cu $\lambda = 1.54$ Å. The scan rate was 1.2°/min, over a diffraction angle 2θ ranging between 2° and 10°. The interlaminar spaces were calculated by the Bragg equation (Liao, Chiu, & Lin, 2010), The CA and nanocomposites samples were performed in a ≈100 μm thick film form.

2.4.2. Differential scanning calorimetry

Thermal analysis experiments were performed using a Mettler Toledo Differential Scanning Calorimeter (DSC) model DSC 822e (Greifensee, Switzerland). The materials were scanned in non-isothermal conditions. Samples of about 8 mg were heated from 20° to 230 °C at 10 °C/min and cooled from 230 °C to 20 °C at 20 °C/min, then heated again from 20 to 230 °C to obtain the glass transition temperature (T_g), melting point (T_m) in the second heating.

Crystallinity (X_c) was calculated from the relationship between the latent fusion heat of the samples analyzed (ΔH_f) and the theoretical latent fusion heat for 100% crystallinity ($\Delta H_f^\circ = 58.8$ J/g) (Cerqueira, Rodrigues, & Assuncao, 2006), according to the equation: crystallinity (%) $= \Delta H_f / \Delta H_f^\circ \times 100$.

2.4.3. Thermogravimetric analysis

Thermogravimetric analysis (TGA) was performed using a SDT 2960 DSC-TGA, TA Instruments (Wilmington, USA), at 20 °C/min, between 0 and 800 °C, in air.

2.4.4. Opacity

Opacity of the nanocomposites was determined using a UV-Vis spectrophotometer Shimadzu UVmini-1240 (Kyoto, Japan). The film samples were cut into a rectangular piece (1.0 cm × 4.5 cm) and placed on the sample compartment of a spectrophotometer. The opacity of films was calculated using: Opacity = Abs_{600}/X (Tunc & Duman, 2010). Where: Abs_{600} = absorbance at 600 nm; X = film thickness (mm).

2.4.5. Surface color measurement

$MtCu^{2+}$/CA film color was measured using a CR 410 Minolta Chroma Meter (Minolta Series, Tokyo, Japan). The CIELAB scale was used, lightness (L) and chromaticity parameters a (red-green) and b (yellow-blue) were measured. A white standard color plate was used as the background for color measurements D65 illuminant and 10° observer was used for analysis (Bruna et al., 2012).

Each analysis was performed in five replicates and results reported the average value. The total color change ΔE were calculated by $\Delta E = [(\Delta L^*)^2 + (\Delta a^*)^2 + (\Delta b^*)^2]^{1/2}$ and the Whitish Indexes were calculated by $Wi = 100 - [(100 - L^*)^2 + a^{*2} + b^{*2}]^{1/2}$ (Quintero et al., 2012).

2.4.6. Mechanical properties

Tensile testing was performed at room temperature on a Zwick Roell (Ulm, Germany) dynamometer model M.BDO-FBO 5HT, according to ASTM D882. Tests were carried out at a cross-head speed of 50 mm/min until breaking.

2.4.7. Oxygen transmission rate (OTR)

The OTR measurements were carried out with an Oxygen Permeation Analyzer (MOCON, Minneapolis, USA) OX-TRAN® MS2/20, equipped with a Coulox® oxygen sensor with a sensitivity of 0.1 [$cm^3/(m^2\ day)$]. The temperature test was 23 °C and relative humidity was 0% according to ASTM D3985. Oxygen permeability (OP) was calculated from OTR data.

2.4.8. Scanning electron microscopy

SEM photographs were taken with a JSM-5410 Jeol Scanning Microscope (Tokyo, Japan), at 10^{-4} Pa, 10 kV in inert atmosphere with 500× and 5000× magnification. The films were previously fractured under liquid nitrogen in preparation for cross-section analysis and coated with gold palladium using a sputtering System Hummer 6.2.

2.4.9. Transmission electron microscopy

TEM micrographs were obtained with a Philips Tecnai 12 (Eindhoven, Holland), with the acceleration voltage of 80 kV. The films were previously supported in a LR-white resin and microtomed by Sorvall MT-5 ultramicrotomy (thick section: 60–80 nm), with 16,500× and 60,000× magnification.

2.4.10. Antimicrobial activity

The antimicrobial nanocomposites effect on the growth of *E. coli* (O157:H7) was also investigated. The antimicrobial activities were performed according ASTM E2149-01. The working bacterial solution containing *E. coli* in sterile buffer solutions grown at optimal growth conditions had a initial concentration of 5.34×10^9 cell/ml, and serial dilutions in buffer solution were carried out, and the microorganism suspensions were plated on LBA. Colonies were quantified in the dilution 1×10^{-6}. First, the material to be tested (1 g) was introduced into test tubes, maintained at 37 °C for 24 h in agitation. Later one hundred microliters of the last solutions were spread onto LBA and incubated on the plates. The colonies were counted (in CFU/ml).

The activity values are expressed as the number of colony forming units/ml. the percentage of inhibition of different antimicrobial films was calculated with the equation established in the standard test method (ASTM E2149-01):

$$\text{Reduction, \%(CFU/ml)} = \frac{B - A}{B} \times 100 \quad (3)$$

where A = CFU per milliliter for the flask containing the treated substrate after the specified contact time and B = "0" contact time CFU per milliliter for the flask used to determine "A" before the addition of the treated substrate.

3. Results and discussion

3.1. X-ray diffraction

Fig. 1 shows the analysis performed of $MtCu^{2+}$, CA and the nanocomposites with different concentrations (1, 3 and 5 wt.% of $MtCu^{2+}$). In all cases, the nanocomposites exhibited two well-defined diffraction peaks (between 2° and 10°), which can only be associated to the interlayer distance ($d001$) of the clay incorporated in the polymer, as pure CA did not present this characteristic peak (Pukanszky, Szamel, Klebert, & Sajo, 2008).

Moreover, the presence of two peaks in the X-ray diffractogram could indicate two different intercalation degrees of CA in the pristine Mt (Fig. 1), the first peak (lower angle) can be due to polymer intercalation in the interlayer of the clay mineral and the second peak can be attributed to a small amount of montmorillonite layers that were not intercalated by CA molecules, similar

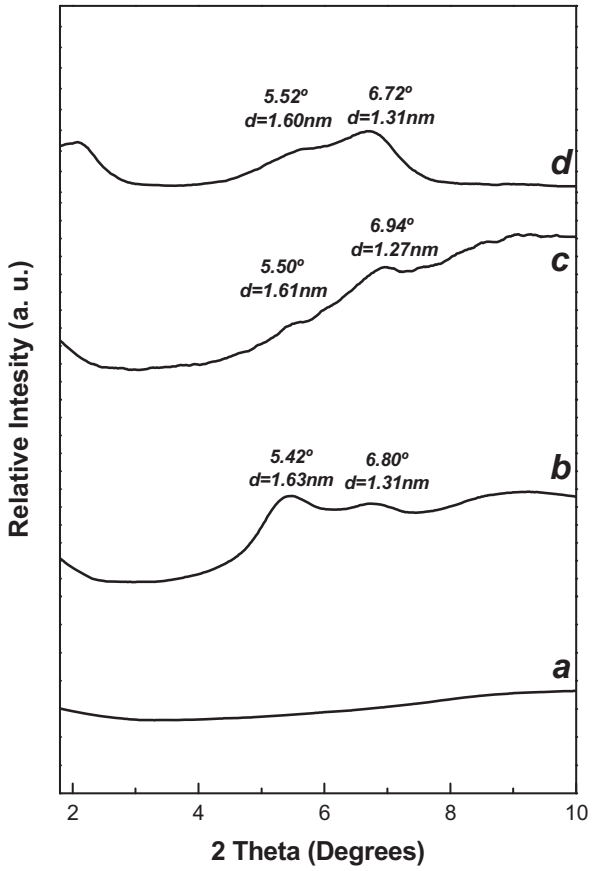

Fig. 1. XRD patterns of (a) CA, (b) 1% $MtCu^{2+}$/CA, (c) 3% $MtCu^{2+}$/CA and (d) 5% $MtCu^{2+}$/CA.

results were obtained by Araujo et al. (2007), introducing organo-montmorillonite modified with genamin into polyethylene.

On the other hand, it is possible to observe that at higher $MtCu^{2+}$ concentration, there is much less intercalation which could be attributed to a mineral clay agglomeration in the nanocomposites, demonstrating the presence of residual layered clay tactoids form in the polymer matrix.

In all the nanocomposites, the peaks presented higher interlaminar distances values (around 1.27–1.63 nm) compared to the value of $MtCu^{2+}$ (1.22 nm) reported in our previous works (Bruna et al., 2012), which is indicating a certain degree of clay intercalation into polymer matrix, as was observed in early studies of Tunc et al., for Mt/methyl cellulose nanocomposites films (Tunc & Duman, 2010)

3.2. Differential scanning calorimeter (DSC)

The effect of adding three different $MtCu^{2+}$ concentrations on the thermal properties of the nanocomposites was evaluated through DSC. Table 1 presents the thermal properties of CA and its nanocomposites: glass transition temperature, T_g, melting temperature, T_m, the heat of fusion due to the CA melting, ΔH_f, and the degree of crystallinity, X_c. As shown in Table 1, the glass transition temperature remains practically unchanged when $MtCu^{2+}$ was added in different concentrations into the CA, indicating that the modified clay is not affecting the amorphous phase of the polymer. A similar trend can be observed in the melting temperatures, where apparently no change was observed when $MtCu^{2+}$ was added. This indicates that the presence of modified clay did not influence the size and the crystal ordering, the same effect was observed by Araujo et al. (2007) that did not find significant differences in the

Table 1
DSC data of CA and $MtCu^{2+}$/CA nanocomposites.

Sample	T_g (°C)	T_m (°C)	ΔH_m (J/g)	Crystallinity (%)
CA	164 ± 2[a]	200 ± 2[a]	0.86 ± 0.08[a]	1.5 ± 0.1[a]
1%$MtCu^{2+}$/CA	164 ± 2[a]	200 ± 4[a]	0.84 ± 0.05[a]	1.4 ± 0.1[a]
3%$MtCu^{2+}$/CA	165 ± 3[a]	204 ± 4[a]	0.52 ± 0.08[b]	0.9 ± 0.1[b]
5%$MtCu^{2+}$/CA	163 ± 3[a]	202 ± 2[a]	0.37 ± 0.12[b]	0.6 ± 0.1[b]

Different letters (a and b) indicate significant differences among the values of the same optical property (three replicates).

melting temperature and the shapes of the melting peaks with the addition of organoclays in polyethylene.

On the other hand, it can be observed that the presence of $MtCu^{2+}$ produced a decreased on the CA crystallization. This effect is due to the fact that $MtCu^{2+}$ presents a certain degree of compatibility with the CA, which is attributed to carbonyl groups from the CA structure coordinate to ionic copper from modified clay (Kim et al., 2001), hindering the movement and arrangement of the polymer chains to its crystallization, being more evident when increasing the amount of $MtCu^{2+}$ added to the polymer. The same effect was observed in studies of Cu/LDPE nanocomposites (Xia, Cai, & Xie, 2006), in which the values of crystallinity decreased when micro- or nanoparticles of copper were added.

3.3. Thermogravimetric analysis

The thermal decomposition behavior of CA and all nanocomposites under air atmosphere is shown in the thermal gravimetric analysis (TGA) and its derivative (DTG) curves (Fig. 2a and b), where it is not observed the presence of water attributed to dehydration (≈100 °C) in all cases, but it is possible to observe two typical thermal degradation processes for this type of polymer which is attributed to fragmentation of macromolecular structure (≈360 °C) and carbonization of products (≈550 °C) to ash (Rodríguez et al., 2012). A new step can be observed in the nanocomposites at ≈300 °C, which could be related to the water associated with the absorbed copper species in the mineral clay (Ding & Frost, 2004; Kloprogge, Mahmutagic, & Frost, 2006).

Moreover, It can be observed that the thermal stability of CA was slightly modified by the presence of $MtCu^{2+}$, which decreased the onset of decomposition of the CA sample from 376 until 370, 366 and 350 °C when it was added 1, 3 and 5 wt.% of modified clay respectively (Table 2), which indicates that the nanocomposites are less thermally stable than pure CA. Similar results were also observed by Gaan et al. (2011), for CA containing bisphosphoramidates.

The decrease in the $MtCu^{2+}$/CA nanocomposites thermal stability when the $MtCu^{2+}$ was added, could be attributed to the presence of Cu^{2+}, because the ionic copper could be acting as a catalyst in the CA hydrolytic depolymerization reaction. This effect has been studied by Su et al. (Zhang et al., 2009), where the addition of $CuCl_2$ with other metal accelerates the rate of cellulose depolymerization. On the other hand, it was observed a slight deacetylation in CA membranes when copper salts were present (Farooque, Al-Amoudi, & Numata, 1999), and a remarkable effect on the deterioration mainly through the scission of a membrane polymer chain, thus reducing both its molecular weight as well as mechanical strength.

This effect has also been observed in other types of polymer, such as styrene–acrylonitrile copolymer (Shen, Wang, Yuan, Guo, & Wu, 2008), where copper ions accelerate its deterioration, in which the degradation mechanism was affected by the presence of $CuSO_4$ when the material were in prolonged contact at a temperature above 230 °C.

3.4. Oxygen permeability

In Fig. 3, a decrease in permeation values is observed when $MtCu^{2+}$ is added to the polymer matrix, reaching a 16% and 28% of decrease in permeability when 1% and 3% of $MtCu^{2+}$ was added, respectively. This is according with the results obtained in Section 3.1, where it was observed that the nanocomposites presented an intercalated morphology of the clays that increases the tortuous pathway for permeating gas molecules (de Azeredo, 2009). However, it is possible to observe that in the nanocomposites with 5% $MtCu^{2+}$ the oxygen permeation increases, which could be related to the $MtCu^{2+}$ agglomeration due to the degree of dispersion of the nano-platelets which are connected to the tortuosity factor and consequently the permeability (Choudalakis & Gotsis, 2009).

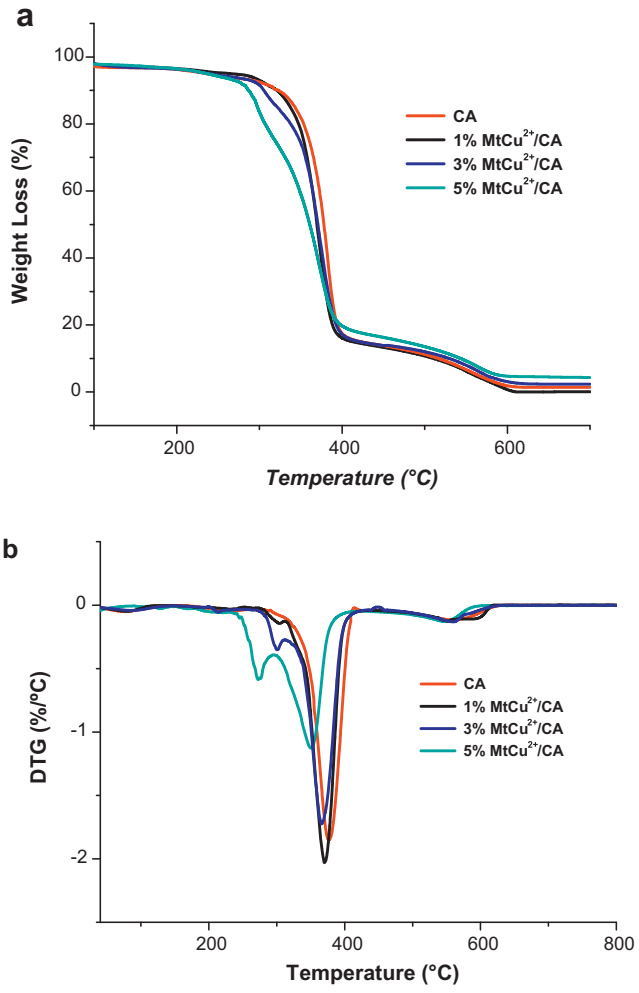

Fig. 2. Thermal gravimetric (TG) and derivate thermogravimetric (DTG) curves of the thermal degradation of CA and its $MtCu^{2+}$/CA nanocomposites with different percentage of $MtCu^{2+}$ nanoparticle content.

Table 2
Thermogravimetric analysis data of pure cellulose acetate and $MtCu^{2+}$/CA nanocomposites.

Sample	Step 1		Step 2	
	Temperature range (°C)	DTG peak (°C)	Temperature range (°C)	DTG peak (°C)
CA	–	–	282–214	376
1%$MtCu^{2+}$/CA	276–312	303	312–409	370
3%$MtCu^{2+}$/CA	276–313	301	313–409	366
5%$MtCu^{2+}$/CA	245–296	274	296–398	350

Table 3
Optical properties of CA and $MtCu^{2+}$/CA nanocomposites.

Sample	L^*	a^*	b^*	ΔE^*	Whitish Index	Opacity
CA	89.9 ± 0.5^a	2.36 ± 0.05^a	-3.57 ± 0.08^a	–	89.0 ± 0.4^a	0.36 ± 0.03^a
1% $MtCu^{2+}$/CA	89.5 ± 0.4^b	1.97 ± 0.5^b	-3.17 ± 0.07^b	1.2 ± 0.5^a	88.9 ± 0.3^b	0.68 ± 0.01^b
3% $MtCu^{2+}$/CA	88.9 ± 0.4^c	1.01 ± 0.06^c	-2.43 ± 0.11^c	3.9 ± 0.6^b	88.6 ± 0.4^c	1.41 ± 0.22^c
5% $MtCu^{2+}$/CA	88.0 ± 0.5^d	0.41 ± 0.12^d	-1.67 ± 0.54^d	7.8 ± 1.9^c	87.8 ± 0.5^d	2.16 ± 0.19^d

Different letters (a–d) indicate significant differences among the values of the same optical property.

Table 4
Mechanical properties of CA and $MtCu^{2+}$/CA nanocomposites.

Sample	Tensile modulus (N/mm^2)	Tensile strength (N/mm^2)	Elongation at break (%)
CA	1178 ± 363^a	37.8 ± 10.0^a	3.1 ± 0.1^a
1%$MtCu^{2+}$/CA	1144 ± 356^a	36.7 ± 7.3^a	2.8 ± 0.3^a
3%$MtCu^{2+}$/CA	1136 ± 270^a	39.4 ± 6.8^a	3.1 ± 0.5^a
5%$MtCu^{2+}$/CA	1133 ± 324^a	31.9 ± 13.6^a	3.5 ± 0.6^b

Different letters (a and b) indicate significant differences among the values of the same mechanics property.

3.5. Optical properties

The results from UV visual spectrometry scan and color measurement are shown in Table 3.

As it was expected, it is possible to observe an increase in the opacity values of the films when increasing the concentration of $MtCu^{2+}$ in the CA matrix, from 0.36 to 2.16. Similar results were observed by Tunc and Duman after the incorporation of Mt in methyl cellulose (Tunc & Duman, 2011). So, this reduction in the amount of light being transmitted through the nanocomposite films could indicates that $MtCu^{2+}$ are not exfoliated (Oksman & Petersson, 2006). It is well-known that the transparency in nanocomposites in general is associated with a good level of exfoliation of the clay in the matrix (Paiva, Morales, & Guimaraes, 2007), because the exfoliated clay does not deflect or reflect the light (de Paiva et al., 2007), as the layers of montmorillonite are smaller than wavelengths of the light.

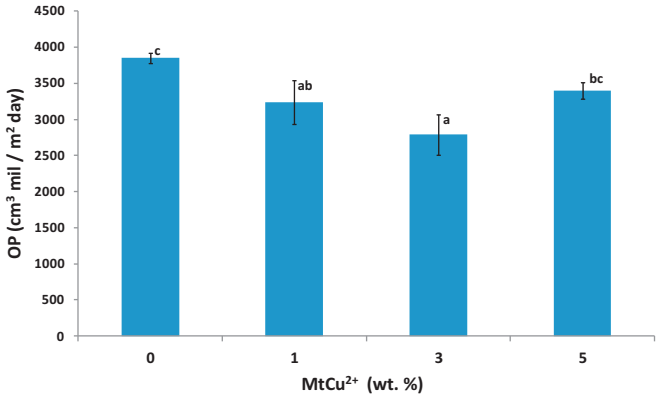

Fig. 3. Effect of $MtCu^{2+}$ content on oxygen permeation (OP) of cellulose acetate nanocomposites. Different letters (a–c) indicate significant differences among the values of the oxygen permeation.

Regarding the color analysis of the films, a significantly lower ($p < 0.05$) Whitish Index can be observed (Table 3) when the amount of $MtCu^{2+}$ was increased in the film. Moreover, the color difference (ΔE) of $MtCu^{2+}$/CA nanocomposites films increased significantly ($p < 0.05$) compared to CA control film, which was caused by development of slight greenish (decrease a^* value) and yellowish (increase in b^* value). Similar results were obtained by introducing this type of nanoreinforcement in LDPE (Bruna et al., 2012).

3.6. Mechanical properties

Table 4 shows the results of tensile testing of $MtCu^{2+}$/CA nanocomposites, determined at a crosshead speed of 50 mm/min. It is possible to observe that the tensile modulus tends to decrease with the incorporation of $MtCu^{2+}$, but this change is not significant ($p < 0.05$), which it can be due to the less uniform distribution of clay particles in the CA matrix (Lima, Pinotti, Felisberti, & Goncalves, 2012). Moreover, the values of elongation at break increased slightly with the 5% $MtCu^{2+}$ addition. This fact would be related to the DSC results, where it was possible to observe a decrease in crystallinity after the addition of the modified clay, suggesting that the amorphous phase of the material would be increasing.

3.7. Scanning and transmission electron microscopy

Fig. 4 shows the morphology of CA and the nanocomposites on the cross-sections. In the SEM images is observed that the surface of CA film presents a homogenous structure without an important presence of pores on the film structure as it has been already reported by Rodríguez et al. (2012). On the other hand, the nanocomposites films presented a more rugged structure on the surface, in which agglomeration clay (white arrows) after an addition of 5% modified clay can be appreciated.

TEM photomicrograph of $MtCu^{2+}$/CA nanocomposite contain 5 wt.% of $MtCu^{2+}$, shown in Fig. 5. It can be seen that the clay is agglomerated in CA (Fig. 5a) corroborating the results obtained in the mechanical properties and SEM. Moreover, it was

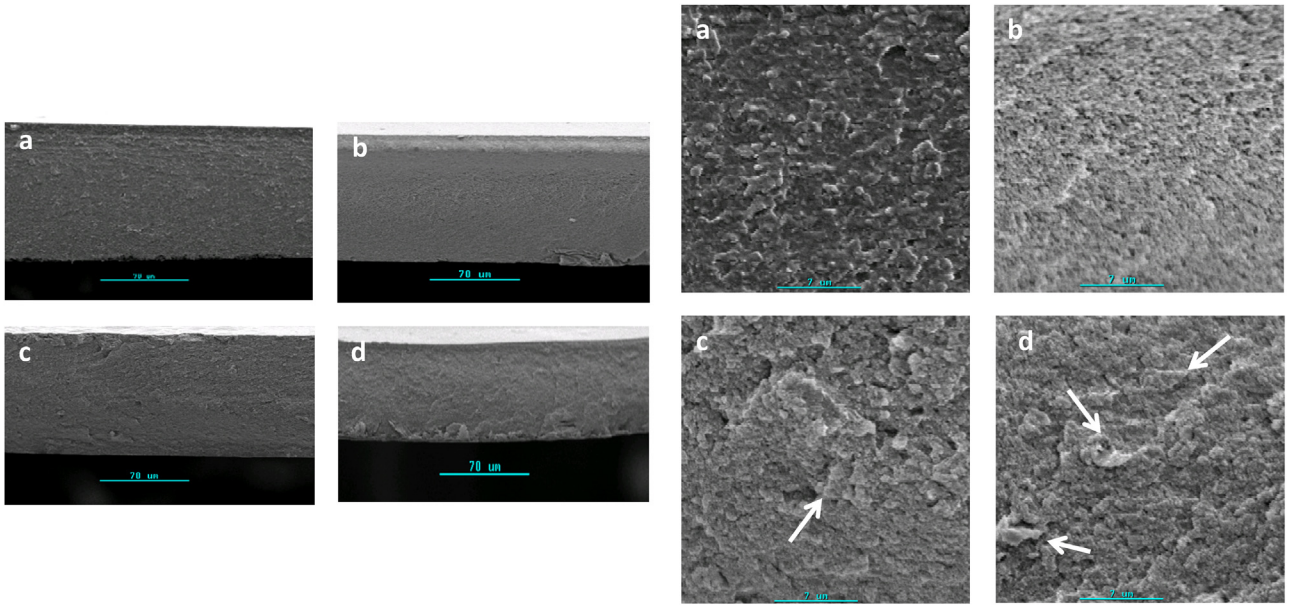

Fig. 4. SEM micrograph of the cross-sections of $MtCu^{2+}$/CA nanocomposites with (a) 0% $MtCu^{2+}$, (b) 1% $MtCu^{2+}$, (c) 3% $MtCu^{2+}$, and (d) 5% $MtCu^{2+}$. Magnification 500× (left) and 5000× (right).

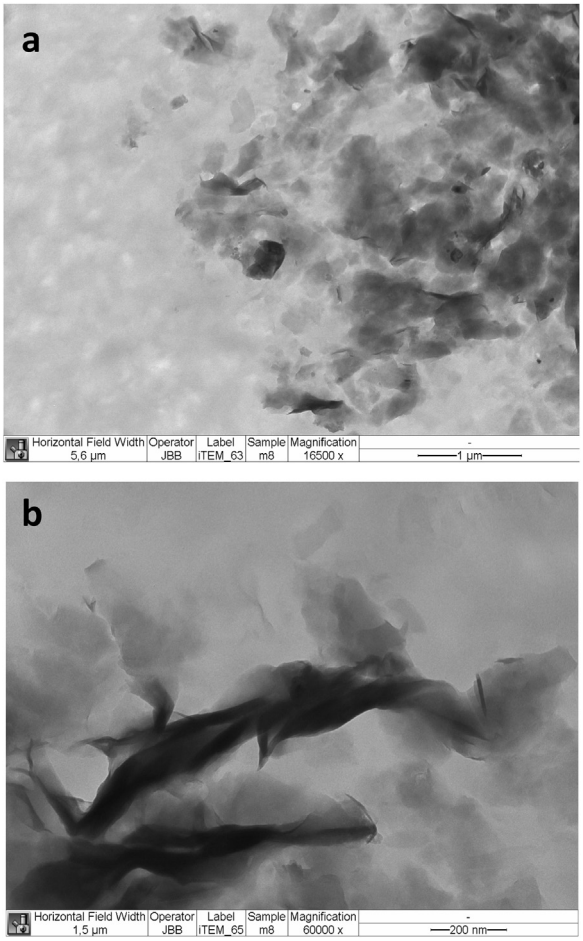

Fig. 5. TEM micrographs of $MtCu^{2+}$/PLA nanocomposite film with 5 wt.% $MtCu^{2+}$: (a) 16,500× and (b) 60,000× magnification.

Table 5
Antimicrobial activity of CA and CA nanocomposites.

Sample	CFU/ml × 10^9 (after contact for 24 h)	Percent reduction of bacteria (%)
1%$MtCu^{2+}$/CA	4.3 ± 0.0	20.3 ± 1.3
3%$MtCu^{2+}$/CA	2.6 ± 0.1	50.6 ± 2.3
5%$MtCu^{2+}$/CA	1.0 ± 0.0	98.0 ± 1.0

possible to observe that the clay is in intercalated and tactoid form (Fig. 5b), which is in agreement with the XRD pattern obtained for the nanocomposite sample.

3.8. Antimicrobial activity

The antimicrobial activity of $MtCu^{2+}$/CA nanocomposites films was tested against *E. coli* by comparing between the initial and the final number CFU after contact with the different nanocomposites. In Table 5, is possible to observe that after the addition of 1% of $MtCu^{2+}$, a 20% of bacteria reduction is obtained, which increases when increasing the $MtCu^{2+}$ concentration in the CA matrix, obtaining a maximum reduction value of 98% when a 5% $MtCu^{2+}$ was added. This efficient bactericidal activity is directly related to the presence of copper in the clay, which is absorbed onto the bacterial cell surface imparting damage to the cell membrane (Raffi et al., 2010).

Comparing these results to those reported in our early works in which a LDPE matrix (Bruna et al., 2012) was used, it is possible to observe the highest antibacterial activity due to a better diffusion of the antimicrobial agent in the CA.

4. Conclusions

In this study $MtCu^{2+}$/CA nanocomposites films were successfully obtained with different $MtCu^{2+}$ concentrations by a casting technique. The nanocomposites films showed intercalated and tactoid structures of modified clay, which were evidenced by DRX and TEM. Moreover, it was possible to observe by SEM certain degree of agglomeration of the clay in the CA matrix. On the other hand, the thermal properties of the nanocomposites showed that

the glass transition and fusion temperatures were unaffected by the $MtCu^{2+}$ addition, but the crystallinity and the thermal stability decreased as $MtCu^{2+}$ content was introduced inside the CA matrix. The nanocomposites films presented an increment in the opacity values compared to CA without nanofiller film, due to the presence of clay in the polymer matrix. The presence of $MtCu^{2+}$ did not present significant changes in the mechanical properties of the material, however, the oxygen permeability decreased according to $MtCu^{2+}$ content until 3 wt.%

Finally, the antimicrobial activity of $MtCu^{2+}$/CA nanocomposite against *E. coli* was very effective, obtaining a 98% reduction of colonies when a 5% of $MtCu^{2+}$ was added to the CA matrix.

In conclusion, considering both the change in the oxygen barrier considering both the change in the oxygen barrier properties as well as antimicrobial activity exhibited by $MtCu^{2+}$/CA nanocomposite films makes it an ideal material to use in food packaging.

Acknowledgements

The authors would like to thank the Comisión Nacional de Investigación Científica y Tecnológica, CONICYT, for its financial support by the Programa Bicentenario de Ciencia y Tecnología (Project PDA-22), at the Programa de Financiamiento Basal para Centros Científicos y Tecnológicos de Excelencia (Project FB0807) and the Fondo Nacional de Desarrollo Científico y Tecnológico (Project FONDECYT de Iniciación 11110518).

References

Araujo, E. M., Barbosa, R., Morais, C. R. S., Soledade, L. E. B., Souza, A. G., & Vieira, M. Q. (2007). Effects of organoclays on the thermal processing of PE/clay nanocomposites. *Journal of Thermal Analysis and Calorimetry*, *90*(3), 841–848.

Arora, A., & Padua, G. W. (2010). Review: Nanocomposites in Food Packaging. *Journal of Food Science*, *75*(1), R43–R49.

Bruna, J. E., Peñaloza, A., Guarda, A., Rodríguez, F., & Galotto, M. J. (2012). Development of $MtCu^{2+}$/LDPE nanocomposites with antimicrobial activity for potential use in food packaging. *Applied Clay Science*, *58*, 79–87.

Cerqueira, D. A., Rodrigues, G., & Assuncao, R. M. N. (2006). A new value for the heat of fusion of a perfect crystal of cellulose acetate. *Polymer Bulletin*, *56*(4–5), 475–484.

Cruz-Romero, M. C., Murphy, T., Morris, M., Cummins, E., & Kerry, J. P. (2013). Antimicrobial activity of chitosan, organic acids and nano-sized solubilisates for potential use in smart antimicrobially-active packaging for potential food applications. *Food Control*, *34*(2), 393–397.

Choudalakis, G., & Gotsis, A. D. (2009). Permeability of polymer/clay nanocomposites: A review. *European Polymer Journal*, *45*(4), 967–984.

de Abreu, D. A. P., Cruz, J. M., & Losada, P. P. (2012). Active and intelligent packaging for the food industry. *Food Reviews International*, *28*(2), 146–187.

de Azeredo, H. M. C. (2009). Nanocomposites for food packaging applications. *Food Research International*, *42*(9), 1240–1253.

de Azeredo, H. M. C. (2013). Antimicrobial nanostructures in food packaging. *Trends in Food Science & Technology*, *30*(1), 56–69.

de Lima, J. A., Pinotti, C. A., Felisberti, M. I., & Goncalves, M. D. (2012). Morphology and mechanical properties of nanocomposites of cellulose acetate and organic montmorillonite prepared with different plasticizers. *Journal of Applied Polymer Science*, *124*(6), 4628–4635.

de Paiva, L. B., Morales, A. R., & Guimaraes, T. R. (2007). Structural and optical properties of polypropylene–montmorillonite nanocomposites. *Materials Science and Engineering A: Structural Materials Properties Microstructure and Processing*, *447*(1–2), 261–265.

Ding, Z., & Frost, R. L. (2004). Thermal study of copper adsorption on montmorillonites. *Thermochimica Acta*, *416*(1–2), 11–16.

Farooque, A. M., Al-Amoudi, A., & Numata, K. (1999). Degradation study of cellulose triacetate hollow fine-fiber SWRO membranes. *Desalination*, *123*(2-3), 165–171.

Gaan, S., Mauclaire, L., Rupper, P., Salimova, V., Tran, T. T., & Heuberger, M. (2011). Thermal degradation of cellulose acetate in presence of bis-phosphoramidates. *Journal of Analytical and Applied Pyrolysis*, *90*(1), 33–41.

Hauser, C., & Wunderlicha, J. (2011). Antimicrobial packaging films with a sorbic acid based coating. *Procedia Food Science*, *1*, 197–202.

Hoenich, N. (2006). Cellulose for medical applications: Past, present, and future. *Bioresources*, *1*(2), 270–280.

Kim, H. S., Kim, Y. J., Kim, J. J., Lee, S. D., Kang, Y. S., & Chin, C. S. (2001). Spectroscopic characterization of cellulose acetate polymer membranes containing Cu(1,3-butadiene) OTf as a facilitated olefin transport carrier. *Chemistry of Materials*, *13*(5), 1720–1725.

Kloprogge, J. T., Mahmutagic, E., & Frost, R. L. (2006). Mid-infrared and infrared emission spectroscopy of Cu-exchanged montmorillonite. *Journal of Colloid and Interface Science*, *296*(2), 640–646.

Liao, Y., Chiu, C., & Lin, J. (2010). General intercalation of poly(oxyalkylene)-amidoacids for anionic and cationic layered clays. *Industrial and Engineering Chemistry Research*, *49*, 5001–5005.

Malachova, K., Praus, P., Rybkova, Z., & Kozak, O. (2011). Antibacterial and antifungal activities of silver, copper and zinc montmorillonites. *Applied Clay Science*, *53*(4), 642–645.

Mohanty, A. K., Park, H. M., Misra, M., & Drzal, L. T. (2004). Green nanocomposites from cellulose acetate bioplastic and clay: Effect of eco-friendly triethyl citrate plasticizer. *Biomacromolecules*, *5*(6), 2281–2288.

Muffler, K., & Ulber, R. (2008). Use of renewable raw materials in the chemical industry – Beyond sugar and starch. *Chemical Engineering & Technology*, *31*(5), 638–646.

Nan, L., Yang, W. C., Liu, Y. Q., Xu, H., Li, Y., Lu, M. Q., et al. (2008). Antibacterial mechanism of copper-bearing antibacterial stainless steel against *E. coli*. *Journal of Materials Science & Technology*, *24*(2), 197–201.

Oksman, K., & Petersson, L. (2006). Biopolymer based nanocomposites: Comparing layered silicates and microcrystalline cellulose as nanoreinforcement. *Composites Science and Technology*, *66*(13), 2187–2196.

Pillai, C. K. S., & Luckachan, G. E. (2011). Biodegradable polymers – A review on recent trends and emerging perspectives. *Journal of Polymers and the Environment*, *19*(3), 637–676.

Pukanszky, B., Szamel, G., Klebert, S., & Sajo, I. (2008). Thermal analysis of cellulose acetate modified with caprolactone. *Journal of Thermal Analysis and Calorimetry*, *91*(3), 715–722.

Puls, J., Wilson, S. A., & Holter, D. (2011). Degradation of cellulose acetate-based materials: A review. *Journal of Polymers and the Environment*, *19*(1), 152–165.

Quintero, R. I., Rodriguez, F., Bruna, J., Guarda, A., & Galotto, M. J. (2012). Cellulose acetate butyrate nanocomposites with antimicrobial properties for food packaging. *Packaging Technology and Science*, http://dx.doi.org/10.1002/pts.1981

Raffi, M., Mehrwan, S., Bhatti, T. M., Akhter, J. I., Hameed, A., Yawar, W., et al. (2010). Investigations into the antibacterial behavior of copper nanoparticles against *Escherichia coli*. *Annals of Microbiology*, *60*(1), 75–80.

Rimdusit, S., Jingjid, S., Damrongsakkul, S., Tiptipakorn, S., & Takeichi, T. (2008). Biodegradability and property characterizations of methyl cellulose: Effect of nanocompositing and chemical crosslinking. *Carbohydrate Polymers*, *72*(3), 444–455.

Risch, S. J. (2009). Food packaging history and innovations. *Journal of Agricultural and Food Chemistry*, *57*(18), 8089–8092.

Rodríguez, F. J., Galotto, M. J., Guarda, A., & Bruna, J. E. (2011). Modification of cellulose acetate films using nanofillers based on organoclays. *Journal of Food Engineering*, http://dx.doi.org/10.1016/j.jfoodeng.2011.1005.1004

Rodríguez, F. J., Galotto, M. J., Guarda, A., & Bruna, J. E. (2012). Modification of cellulose acetate films using nanofillers based on organoclays. *Journal of Food Engineering*, *110*, 262–268.

Shen, F., Wang, Y. M., Yuan, X. F., Guo, W. H., & Wu, C. F. (2008). Interfacial coordination reaction in copper sulfate particles filled styrene–acrylonitrile copolymer composites. *Journal of Macromolecular Science Part B: Physics*, *47*(1), 76–86.

Sozer, N., & Kokini, J. L. (2009). Nanotechnology and its applications in the food sector. *Trends in Biotechnology*, *27*(2), 82–89.

Tang, X. Z., Kumar, P., Alavi, S., & Sandeep, K. P. (2012). Recent advances in biopolymers and biopolymer-based nanocomposites for food packaging materials. *Critical Reviews in Food Science and Nutrition*, *52*(5), 426–442.

Tunc, S., & Duman, O. (2010). Preparation and characterization of biodegradable methyl cellulose/montmorillonite nanocomposite films. *Applied Clay Science*, *48*(3), 414–424.

Tunc, S., & Duman, O. (2011). Preparation of active antimicrobial methyl cellulose/carvacrol/montmorillonite nanocomposite films and investigation of carvacrol release. *LWT: Food Science and Technology*, *44*(2), 465–472.

Xia, X. P., Cai, S. Z., & Xie, C. S. (2006). Preparation, structure and thermal stability of Cu/LDPE nanocomposites. *Materials Chemistry and Physics*, *95*(1), 122–129.

Yoksan, R., & Yokesahachart, C. (2011). Effect of amphiphilic molecules on characteristics and tensile properties of thermoplastic starch and its blends with poly(lactic acid). *Carbohydrate Polymers*, *83*(1), 22–31.

Zhang, Z. C., Yu, S., Brown, H. M., Huang, X. W., Zhou, X. D., & Amonette, J. E. (2009). Single-step conversion of cellulose to 5-hydroxymethylfurfural (HMF), a versatile platform chemical. *Applied Catalysis A: General*, *361*(1–2), 117–122.